

Influence of gadolinium doping on low- and high-order nonlinear optical properties and transient absorption dynamics of ZnO nanomaterials

Mottamchetty Venkatesh^a, Rashid A. Ganeev^{a,**}, Konda Srinivasa Rao^a, Ganjaboy S. Boltaev^a, Ke Zhang^a, Amit Srivastava^c, Jasleen K. Bindra^{c,d}, Subhash Singh^{a,b}, Vyacheslav V. Kim^a, Sandeep Kumar Maurya^a, Geoffrey F. Strouse^c, N.S. Dalal^c, Chunlei Guo^{a,b,*}

^a The Guo China-US Photonics Laboratory, State Key Laboratory of Applied Optics, Changchun Institute of Optics, Fine Mechanics and Physics, Chinese Academy of Sciences, Changchun, 130033, China

^b The Institute of Optics, University of Rochester, Rochester, NY, 14627, USA

^c Department of Chemistry and Biochemistry, Florida State University, Tallahassee, FL, 32306, USA

^d Department of Physics, TDPG College, VBS Purvanchal University, Jaunpur, 222001, India

ABSTRACT

Doping of materials by suitable additives can dramatically modify the physical characteristics of the complex systems. In this paper, we investigate the role of gadolinium concentration on the linear, nonlinear optical properties and transient absorption dynamics of ZnO and Al-doped ZnO. The characteristics of the mentioned materials with different dopant concentrations are evaluated using absorption spectroscopy, Z-scan and pump-probe technique with femtosecond laser pulses at 800 and 400 nm wavelengths. The nonlinear absorption is increased in Al-doped ZnO compared to pure ZnO at 800 nm wavelength. Gadolinium dopant demonstrated a significant reduction in nonlinear refractive index and absorption of Al-doped ZnO but could not influence pure ZnO. The transient absorption dynamics of ZnO and Al-doped ZnO illustrated the decrease of response time with dopant concentration. We also generated high-order harmonics using nanosecond heating pulses to generate laser plasmas and femtosecond driving pulses propagating through the plasmas. Laser plasma was generated from an ablated Gd-doped ZnO and the high-order harmonics were studied by varying the delay between heating and driving pulses.

1. Introduction

Investigation of optical nonlinearities in nanostructured semiconductor materials is important which determines their applications in optoelectronic switching, optical data storage, semiconductor optical amplifiers and construction of lasers [1–5]. The future of high-speed optical data communication networks relies on the speed and capacity of optical switching devices [4]. The speed of operation of these photonic devices depends on the light intensity-induced changes in the refractive index of semiconductor materials being used in these devices [5,6]. The mechanisms those responsible for light induced change in refractive index, are (i) the increase in concentration of free carriers due to multi-photon absorption ($n\hbar\nu \geq \Delta E_g$; where ΔE_g is the band gap of semiconductor), and (ii) the Kerr effect, which occurs when the bound charges are excited by photons with energy lesser than the band gap width. Light-induced change in refractive index, saturable absorption (SA), and reverse saturable absorption (RSA) depend on the band gap and the initial concentration of free carriers in semiconductor. Doping

of impurity atoms in nanocrystals of semiconductors, as well as making heterostructures such as core-shell nanoparticles (NPs) and quantum dots allow to control the band gap, and hence, the initial and the light-induced concentration of free charge carriers.

One-dimensional ZnO nanostructures, with coupled semiconducting and piezoelectric properties, have been extensively investigated and widely used to fabricate nanoscale optoelectronic devices. A metal-insulator-semiconductor (Pt/Al₂O₃/ZnO) based self-powered photodetector has been studied in Ref. [7]. In Ref. [8], a distinctive strain-gating method was proposed to manipulate 2D WSe₂-1D ZnO Van der Waals interfacial charge and modulate its photosensing performance by tuning electronic states of WSe₂. Recent developments in 1D ZnO nanostructure based photodetectors and device performance enhancement by strain engineering piezoelectric polarization and interface modulation were reviewed extensively by Zhang et al. [9]. They emphasized a fundamental understanding of electrical and optical phenomena, interfacial and contact behaviours, and device characteristics.

The dopants like gadolinium alter the structural parameters such as

* Corresponding author. The Guo China-US Photonics Laboratory, State Key Laboratory of Applied Optics, Changchun Institute of Optics, Fine Mechanics and Physics, Chinese Academy of Sciences, Changchun, 130033, China.

** Corresponding author. The Guo China-US Photonics Laboratory, State Key Laboratory of Applied Optics, Changchun Institute of Optics, Fine Mechanics and Physics, Chinese Academy of Sciences, Changchun, 130033, China.

E-mail addresses: rashid@ciomp.ac.cn (R.A. Ganeev), guo@optics.rochester.edu (C. Guo).

<https://doi.org/10.1016/j.optmat.2019.109241>

Received 22 May 2019; Received in revised form 10 June 2019; Accepted 7 July 2019

0925-3467/ Published by Elsevier B.V.

crystallite size, lattice constants, stress-strain mechanisms, etc., and hence related nonlinear optical properties [10–12]. Like most of the rare earths, gadolinium is used as a phosphor in various applications [13–19]. Gadolinium is also used for making gadolinium yttrium garnets, as well as various optical components and magneto-optical films [20]. Earlier, the nonlinear optical properties of Gd:ZnO thin films were analyzed by irradiating with electron beam of various dosages, eventually lead to a significant increase in third-order nonlinear optical susceptibility [9]. Aluminum is also used for the reduction of surface resistivity of ZnO and it is termed as AZO [21].

ZnO doped with suitable metals, exhibit good magnetic and optical properties those responsible for device applications. Gd which is selected as a dopant in the present research work belongs to lanthanum group. Gd tremendously modify the electrical and optical properties of ZnO nanocrystals. Gd-doped ZnO allows fabrication of fast spin LEDs, chemical sensors, novel microprocessors, and sensitive biological sensors etc. In this report, we investigated the low-order nonlinear optical characteristics and transient absorption of ZnO and AZO with different concentrations of Gd dopant. In addition, high-order harmonic generation (HHG) is performed using laser ablation of pure ZnO and Gd-doped ZnO.

2. Experimental details

2.1. Preparation of samples

In a typical process, acetylacetonate(acac) passivated nanocrystals were synthesized by the decomposition of zinc undecylena [Zn(UND)_2] with gadolinium (III) 2–4 pentanedionate, dissolved in Hexadecylamine (HDA) using CEM Discover microwave operating under single mode with continuous power at 2.94 GHz. The CEM MW cavity was commercially modified by CEM with a Teflon insert to allow sustainable heating at 300 °C.

In order to synthesize zinc oxide and Gd doped ZnO nanocrystals (GZO), a glass microwave reactor vessel was loaded with appropriate amount of Zn(UND)_2 , Gd(acac)_3 and HDA(4 ml). The microwave (MW) vessel was sealed, and the reactants were kept in water bath at 60 °C for 30 min under continuous stirring, which helped the solids to get dissolved properly. The MW vessel was then inserted into the microwave cavity and heated to 280 °C temperature for 10 min. The solution was allowed to cool down to 50 °C, which was followed by precipitation of nanocrystals using addition of methanol (~5 ml). The product was isolated by the centrifugation and washed with toluene and acetone for four times to remove organic residue. The resultant product was dried overnight under vacuum and stored in clean sealed plastic containers for measurements. Similarly, aluminum doped zinc oxide (AZO) and Gd doped AZO (GAZO) nanocrystals were synthesized by adding Al(acac)_3 salt powder into aforementioned reaction mixture for the synthesis of ZnO and GZO by keeping other experimental parameters constant.

Nanopowders were ultrasonically dispersed into twice distilled water to form a colloidal suspension for the optical measurements. PerkinElmer Lambda 365 double beam spectrophotometer was used for optical absorption measurements in the spectral range of 200–1100 nm. Crystalline properties and lattice constants of samples of nanopowder were measured using PAN analytical X-ray diffractometer with $\lambda = 1.5406 \text{ \AA}$ line from Cu-K α source.

2.2. Experimental method of Z-scan

The conventional Z-scan technique was employed to study the nonlinear optical properties of the ultrasonically dispersed in double distilled water ZnO and AZO. Experimental schematic of Z-scan technique in closed aperture (CA) and open aperture (OA) configurations is shown in Fig. 1(a). Ti: Sapphire laser (Spectra-Physics, Spitfire Ace) provides ultrafast pulses of durations 30 fs with a central maximum at 800 nm and at a repetition rate 1 kHz. A convex lens of focal length

~40 cm was used to focus the laser beam into a quartz cell (of thickness 2 mm) that holds the samples. The cell was moved along the direction of beam propagation.

The transmitted beam was collected by detectors (silicon photodiode, Thorlabs PDA100A-EC) directly through an aperture for OA and CA schemes. The OA measurements were performed using laser light reflected from glass slide and allowed measurement of the nonlinear absorption of samples. In the case of CA, the iris was closed to allow the propagation of 10% of input radiation. The OA and CA schemes were used for determination of two-photon absorption (2PA) coefficients (β) and nonlinear refractive (NR) indices (γ), respectively using 800 and 400 nm laser radiation. 400 nm laser beam was obtained using a barium borate (BBO) crystal to study the role of laser wavelength on the nonlinear optical properties of the sample. Here, Z-scan experiment and the validity of the obtained data depend on the profile of the input laser beam which must be a Gaussian. The profile of the laser beam utilized in the current experimental study was characterized by a CCD camera (Thorlabs). It was evident that the profile is very close to a Gaussian. The full width at half maximum and $1/e^2$ of measured for the 30 fs laser pulses at 800 nm wavelength was 38 and 72 μm , respectively.

2.3. Experimental procedure of pump probe studies

The transient dynamics of ZnO was studied using the non-collinear degenerate pump-probe technique as illustrated in Fig. 1(b). The femtosecond laser pulses of duration ~30 fs at a central wavelength ~400 nm were utilized for this study. Upconversion of laser beam at 800 nm using a BBO crystal (2 mm thickness) generate laser beam of wavelength 400 nm. The reflected and the transmitted beams from beam splitter were used as probe and pump for the study. A motorized stage is employed in the study to introduce a required delay between pump and probe pulses. The relative intensities, diameters of pump and probe beams were kept approximately ~10:1 and 1:2, respectively, throughout the experiment. The transmitted probe beam intensity was measured by a photodiode and its output was connected to a lock-in amplifier. The pump-probe signal is obtained by measuring the transmitted probe beam signal from sample using lock-in amplifier as a function of the delay between the pump and probe beams. Transient absorption study of deionized water was also performed to remove the influence of water from the data on transient absorption of ZnO nanoparticles in water.

2.4. Experimental arrangements of higher harmonic generation(HHG)

The experimental scheme for HHG is shown in Fig. 1(c). The studied samples were ablated by nanosecond pulses (1064 nm, 5 ns, 10 Hz; Q-Smart, Coherent) to create the plasma plume. The driving femtosecond pulses (800 nm, 30 fs, 1 kHz; Spitfire Ace, Spectra Physics) propagated through the plasma at different delays after the beginning of irradiation of target by nanosecond heating pulses. The variable delay (0–10⁶ ns) between 5 ns heating pulses and 30 fs driving pulses was available during generation of harmonics in plasma at the used geometry of experiments when the 800 nm fs pulses were focused inside the plasma from the orthogonal direction with regard to the ablating radiation, at a distance of ~200 μm above the target surface. The generated harmonics emission were directed to the XUV spectrometer containing a cylindrical mirror and a 1200 grooves/mm flat field grating with variable line spacing. The extreme ultraviolet (XUV) spectrum was recorded by a micro-channel plate (MCP) with phosphor screen, and the harmonics were imaged by a CCD camera.

3. Results and discussion

3.1. Characterization of samples

Fig. 2(a) shows the UV–visible spectra of ZnO and AZO as a function

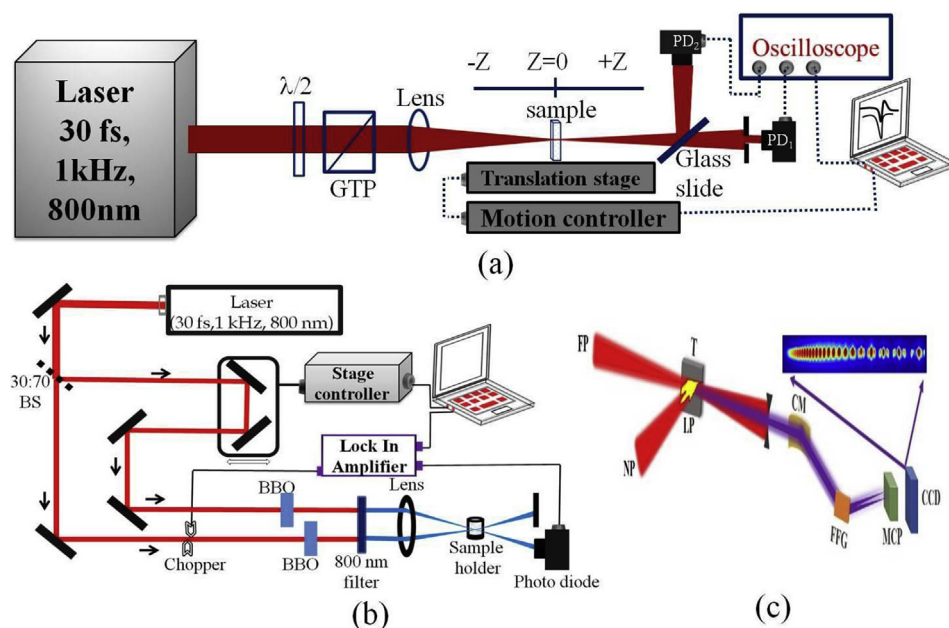


Fig. 1. Experimental schematic of (a) Z-scan scheme. $\lambda/2$, half wave plate; GTP, Glan Thompson Polarizer; PD₁ and PD₂, photodiodes. (b) Pump-probe scheme. BS, beam splitter. (c) High-order harmonic generation setup. FP, driving femtosecond pulses; NP, heating nanosecond pulses; T, target; LP, laser plasma; CM, cylindrical gold-coated mirror; FFG, flat field grating; MCP, microchannel plate; CCD, CCD camera. Inset: Image of the spectrum of high-order harmonics. (For interpretation of the references to colour in this figure legend, the reader is referred to the Web version of this article.)

of concentration of Gd. The ZnO, AZO, AZO + 1% Gd, AZO + 12.5% Gd and ZnO + 20% Gd samples have shown the absorption peaks at 354 (3.50 eV), 356 (3.48 eV), 358 (3.46 eV), 366 (3.38 eV) and 369 (3.36 eV) nm, respectively. These measurements demonstrated that the band gap of ZnO and AZO materials is decreasing with the increasing concentration of Gd. The addition of 20% Gd to ZnO shifted the absorption peak to larger wavelengths by 15 nm compared to pure ZnO. Thus the doping of ZnO and AZO by Gd led to the red shift of absorption peak. Moreover, the doping of ZnO (i.e. AZO) by Al had no effect of shifting the absorption peak.

X-ray diffraction (XRD) patterns of ZnO, GZO, AZO and GAZO nanocrystals (NCs) are presented in Fig. 2(b). XRD results corresponding to AZO and GAZO were scaled by 1.5X and 6X, respectively, for better visualization. Diffraction peaks observed in the 2θ range of 30–80° were indexed for (100), (002), (101), (102), (110), (103), (112), (201) and (202) planes of zinc oxide with wurtzite crystal structure (space group $p63mc$, JCPDS no. 36–1451). The diffraction peak corresponding to (102) plane has been fitted to Gaussian (Fig. 2(c)) in order to investigate the influence of doping on crystalline size and lattice constant of ZnO NCs.

The XRD peak shifts towards smaller 2θ value in doped sample show the increase in lattice parameters. Intensity decrease for most of the diffraction peaks in doped samples demonstrates a decrease in crystalline quality of materials. High amount of impurity doping causes

lattice disorder that can generate stress in the crystal. XRD peaks corresponding to (100) and (002) are used to calculate lattice parameters using expressions $a = b = \lambda / \sqrt{3} \cdot \sin\theta_{100}$ and $c = \lambda / \sin\theta_{002}$; where $\lambda = 1.5406 \text{ \AA}$ is the wavelength of Cu-K α line used for XRD measurements. Scherrer's formula $D = k\lambda / \mu\cos\theta$; where μ is full-width at half maximum (FWHM) of X-ray line, is used to calculate crystalline sizes of different samples of zinc oxides. Lattice parameters and crystalline size for all samples are presented in Table 1. It is interesting to note that lattice parameter is increased by Gd and Al doping in ZnO, while Gd doping in AZO significantly decreases the crystalline size.

To analyze the influence of doping on the surface morphology of zinc oxide NCs, Scanning electron microscopic study was carried out. Fig. 3 presents the SEM images of different zinc oxide samples. Among all, it has been found that NCs in each sample showed a tendency to get self-assembled which in turn become large aggregates of crystals. Gd doping had little influence on surface morphology, but aluminum doping significantly increased the rate of aggregation resulting in clusters with larger size.

Transmission electron microscope (TEM) images of different ZnO samples are presented in Fig. 4. TEM images depict that ZnO and GZO particles are almost spherical in shape with NPs with a range of 10–20 nm. Though the small NPs self-assembled to form larger clusters, individual NPs can be easily identified. In contrast to this, Al doping led to the formation of non-spheroid particles and increases the rate of aggregation and the degree of self-assembly.

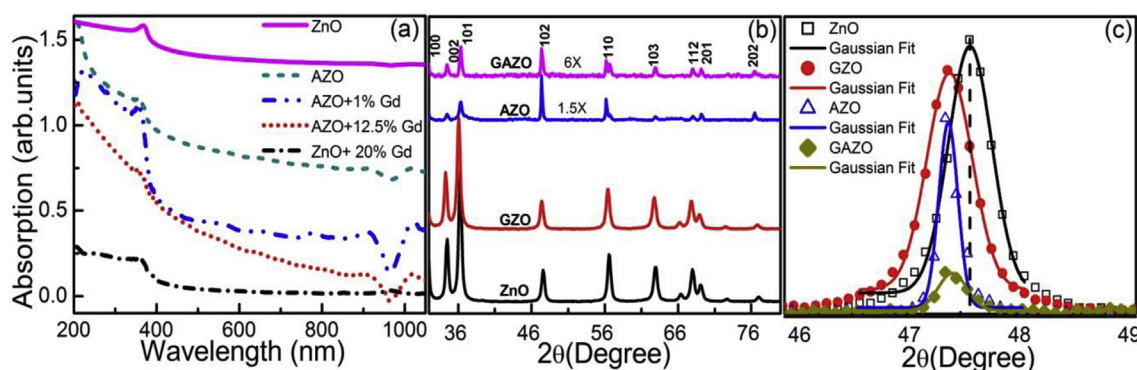


Fig. 2. (a) UV-visible spectra (b) XRD data of undoped Zinc oxide, 12.5% Gd doped zinc oxide (GZO), aluminum doped zinc oxide (AZO) and 12.5% Gd doped AZO. XRD intensity for AZO and GAZO is scaled by 1.5X and 6X respectively. (c) Zoomed view of (102) XRD peak for different zinc oxide samples without scaling.

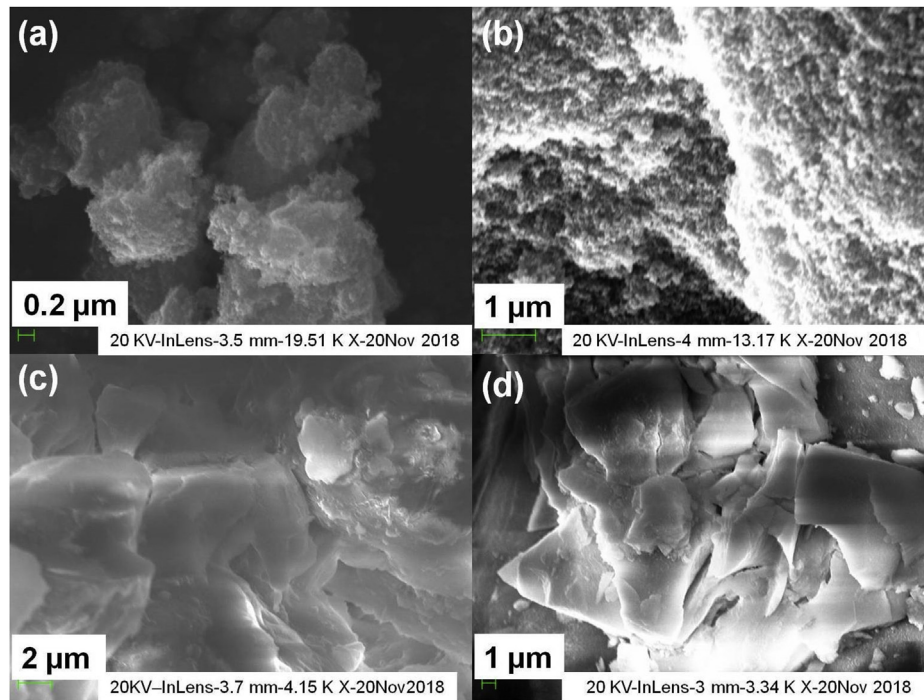


Fig. 3. SEM images of (a) ZnO (scale bar 200 nm) (b) GZO (scale bar 1 μm) (c) AZO (scale bar 2 μm) and GAZO (scale bar 1 μm).

Table 1

Lattice parameters and crystalline size of different zinc oxide samples.

S.No.	Sample	Lattice parameter (\AA)	Crystalline size (\AA)
1	ZnO	$a = b = 3.246; c = 5.199$	9.35 ± 0.019
2	GZO	$a = b = 3.27; c = 5.225$	9.73 ± 0.037
3	AZO	$a = b = 3.239; c = 5.196$	22.18 ± 0.087
4	GAZO	$a = b = 3.239; c = 5.201$	14.28 ± 0.038

3.2. Z-scan measurements of pure and doped ZnO

The nonlinear optical properties of materials were measured using the Z-scan technique by 800 and 400 nm, 30 fs, 1 kHz pulses. There is no absorption at 800 nm in these materials hence it is a non-resonant wavelength. The β , I_{sat} and γ were measured using OA and CA schemes, respectively. The normalized transmittances T_{2PA} and T_{SA} in the cases of 2 PA and SA can be written as follows [22,23]:

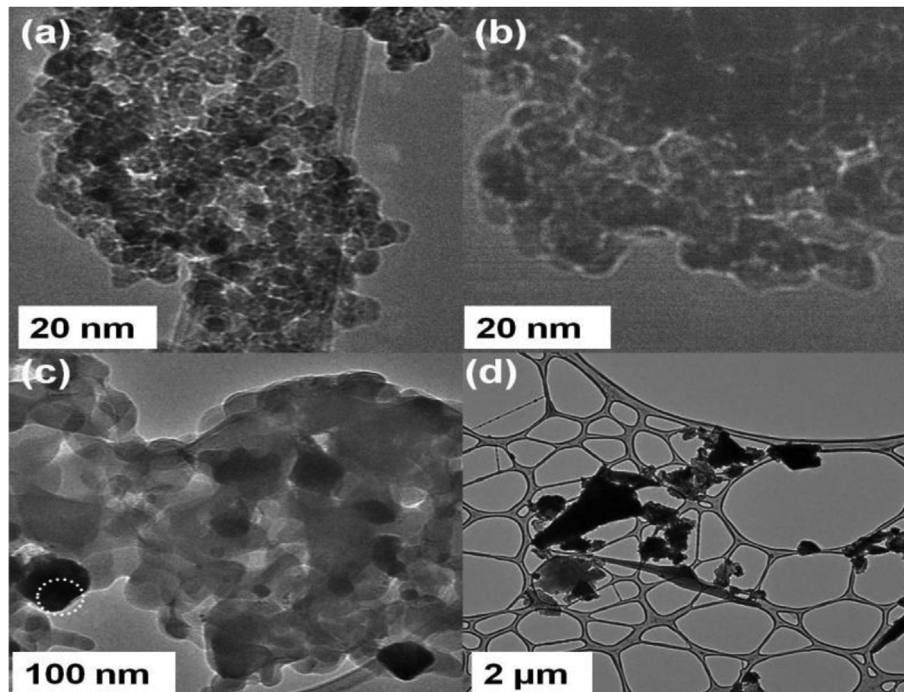


Fig. 4. TEM images of (a) ZnO (b) GZO, (c) AZO, and (d) GZO NCs.

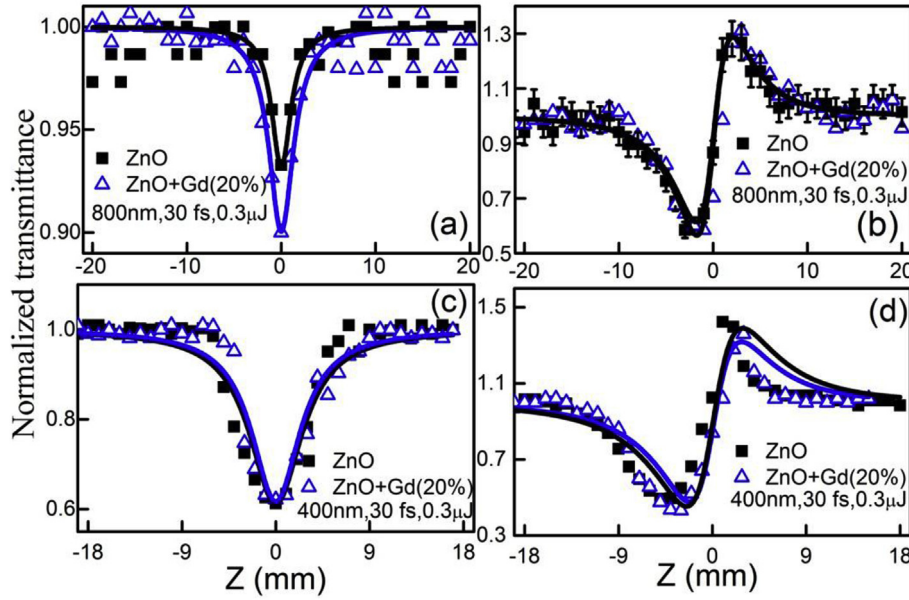


Fig. 5. Z-scans of ZnO and ZnO + Gd (20%). (a) OA Z-scans and (b) CA Z-scans using 800 nm radiation. (c) OA Z-scans and (d) CA Z-scans using 400 nm radiation. Solid curves correspond to theoretical fits.

$$T_{2PA}(z) = \frac{\ln(1+r)}{r} \approx 1 - \frac{r}{2\sqrt{2}} \quad (1)$$

$$T_{SA}(z) = 1 + I/(1+x^2) \quad (2)$$

Here, $r = \beta I_0 L_{eff}/(1+(z/z_0)^2)$, $x = z/z_0$, $z_0 = k(w_0)^2/2$ is the Rayleigh length, k is the wave number $k = 2\pi/\lambda$, w_0 is the beam waist, $I = I_0/I_{sat}$, I_0 is the peak intensity of input beam at focal plane, $L_{eff} = [1 - \exp(-\alpha_0 L)]/\alpha_0$ is the effective length of the medium, α_0 is the linear absorption coefficient and L is the sample thickness. I_{sat} is the saturation intensity, which is related to the concentration of the samples. In the case of CA scheme, the nonlinear refraction and absorption (NRA) induced transmittance is written as [24].

$$T_{NRA}(z) = 1 + \frac{2(-\delta x^2 + 2x - 3\delta)}{x^4 + 10x^2 + 9} \Delta\phi_0 \quad (3)$$

Here $\delta = \beta/2k\gamma$ and $\Delta\phi_0 = k\gamma I_0 L_{eff}$ represents the nonlinear refraction-induced phase change. The nonlinear optical coefficients of 2 PA, SA, NRA and SA + NR processes can be calculated using Eqs. (1)–(3).

Fig. 5(a) and 5(b) show the OA and CA Z-scans of ZnO and ZnO + Gd (20%) using 800 nm, 30 fs pulses, 0.3 μ J pulses. The solid curves represent the theoretical fits of experimental data. The nonlinear optical parameters of these materials are calculated and comprised in Table 2. In OA scheme ZnO and ZnO + Gd (20%) suspensions show

Table 2

Nonlinear optical parameters of ZnO and AZO with different concentrations of Gd.

Material	Laser parameters (Pulse width = 30 fs, Repetition rate = 1 kHz)		Nonlinear refractive index ($10^{-15} \text{ cm}^2 \text{ W}^{-1}$)	Nonlinear absorption coefficient ($10^{-11} \text{ cm}^2 \text{ W}^{-1}$)
	Wavelength (nm)	$I_0 (10^{11} \text{ W cm}^{-2})$		
ZnO	800	1.2	0.95	0.43
	400	1.2	0.66	2.4
ZnO + Gd (20%)	800	1.2	1.0	0.63
	400	1.2	0.59	2.4
AZO	800	0.6	0.56	—
	800	1.2	0.7	1.5
AZO + Gd (12%)	800	1.2	0.47	0.3

nonlinear absorption ($\beta \approx 4.3 \times 10^{-12}$ and $6.4 \times 10^{-12} \text{ cm}^2 \text{ W}^{-1}$). Thus the nonlinear absorption in Gd doped ZnO (20%) was larger than pure ZnO. In the case of CA, the combined processes of 2 PA and NR were observed in two samples that was accompanied by larger valleys compared to peaks. The nonlinear refraction in doped and undoped ZnO was almost the same (i.e. $0.95 \times 10^{-15} \text{ cm}^2 \text{ W}^{-1}$ and $1.0 \times 10^{-15} \text{ cm}^2 \text{ W}^{-1}$).

Fig. 5(c) and 5(d) show the OA and CA Z-scans of ZnO and ZnO + Gd (20%) measured using 400 nm, 30 fs, 0.3 μ J pulses. In OA scheme ZnO and ZnO + Gd (20%) showed the nonlinear absorption attributed to reverse saturable absorption (RSA), which was stronger compared to results of measurement using 800 nm pulses. The nonlinear absorption coefficients of ZnO and ZnO + Gd (20%) at 400 nm were $2.4 \times 10^{-11} \text{ cm}^2 \text{ W}^{-1}$. The growth of β was due to the proximity of incident laser wavelength to the absorption peak of these materials at 360 nm. In the case of CA, the combined processes of RSA and NLR were observed in both samples. The values of γ were determined to be 0.66 and $0.59 \times 10^{-15} \text{ cm}^2 \text{ W}^{-1}$ for ZnO and ZnO (20%Gd), respectively. Our results showed that at 400 nm, doping of Gd slightly reduce the nonlinear refraction compared with pure ZnO, whereas the nonlinear absorption remained unaffected.

Fig. 6(a) and 6(b) show the OA and CA Z-scans of pure AZO measured using 800 nm, 30 fs pulses, at $E = 0.18 \mu\text{J}$ ($I_0 \approx 0.7 \times 10^{11} \text{ W cm}^{-2}$) and 0.3 μJ ($I_0 \approx 1.2 \times 10^{11} \text{ W cm}^{-2}$), respectively. In OA scheme, AZO showed 2 PA, and its β value was $1.5 \times 10^{-11} \text{ cm}^2 \text{ W}^{-1}$. In CA scheme, the combined processes of RSA and NR were observed at higher pulse energies. At 0.18 μJ , AZO exhibited pure self-focusing, whereas at 0.33 μJ it showed the combination of 2 PA and positive NR. The γ at 0.7×10^{11} and $1.2 \times 10^{11} \text{ W cm}^{-2}$ intensities were calculated to be 5.6×10^{-16} and $7.0 \times 10^{-16} \text{ cm}^2 \text{ W}^{-1}$, respectively. At 800 nm probe pulses, γ slightly increased for AZO with the increase in intensity, which is the sign of additional high-order nonlinear refractive mechanism.

Fig. 6(c) and 6(d) show the OA and CA Z-scans of AZO + Gd (12.5%) measured using 800 nm, 30 fs, 0.3 μ J pulses. In OA scheme, AZO + Gd (12.5%) demonstrated 2 PA and its β ($3 \times 10^{-12} \text{ cm}^2 \text{ W}^{-1}$) was very less compared to pure AZO ($15 \times 10^{-12} \text{ cm}^2 \text{ W}^{-1}$). Thus Gd leads to decreasing the nonlinear absorption of AZO at this wavelength. In the case of CA, the combined processes of 2 PA and NLR were observed in 12.5% Gd doped AZO ($\gamma = 4.7 \times 10^{-16} \text{ cm}^2 \text{ W}^{-1}$). The

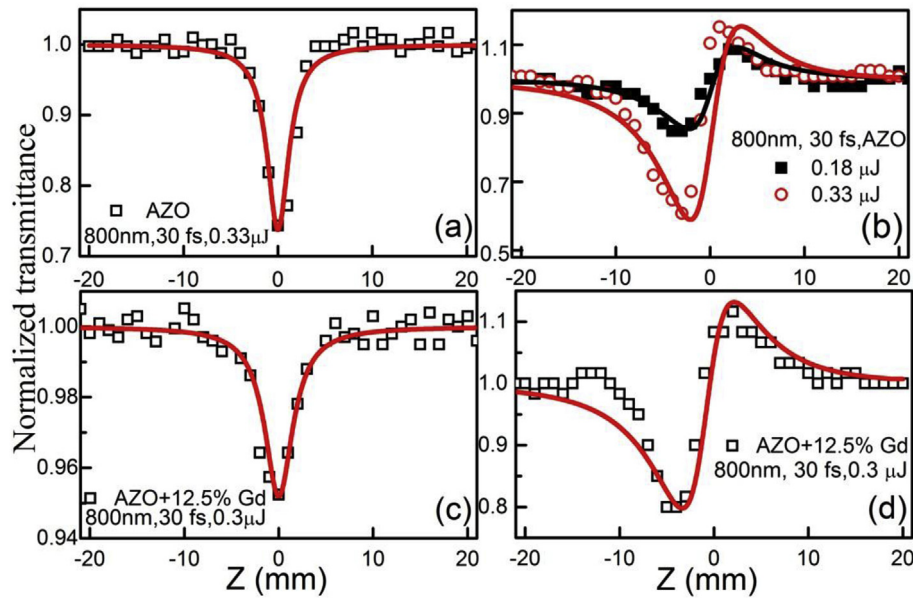


Fig. 6. Z-scans of AZO [(a) OA Z-scan, (b) CA Z-scan] and AZO + 12.5% Gd [(c) OA Z-scan, (d) CA Z-scan] using 800 nm radiation.

measured nonlinear optical parameters are shown in Table 2.

3.3. Pump-probe studies of transient absorption

The transient absorption dynamics of ZnO and AZO at different Gd dopant concentrations was studied using 400 nm, 35 fs laser pulses. Fig. 7 shows the probe pulse transmittance through the materials with variable delay between pump and probe pulses. The experimental data was fitted with double exponential decay equation [25]:

$$\Delta T = A_1 e^{-t/\tau_1} + A_2 e^{-t/\tau_2} \quad (4)$$

Here τ_1 and τ_2 are the relaxation time constants, and A's are the weighing factors. The relaxation time constants of materials with different concentrations of Gd are illustrated in Fig. 8.

The double exponential function demonstrates two decay times involved in sample's relaxation process. The time constant τ_1 is associated with the pulse width of the employed laser pulse (30 fs). Another time constant τ_2 was attributed to the electron thermalization process due to non-resonant excitation at employed pump pulse energy of 400 nm radiation [26]. The relaxation processes occur at the femtosecond time scale. The relaxation time τ_2 was observed to be approximately the same for both ZnO (150 fs) and AZO (153 fs). This shows that there is

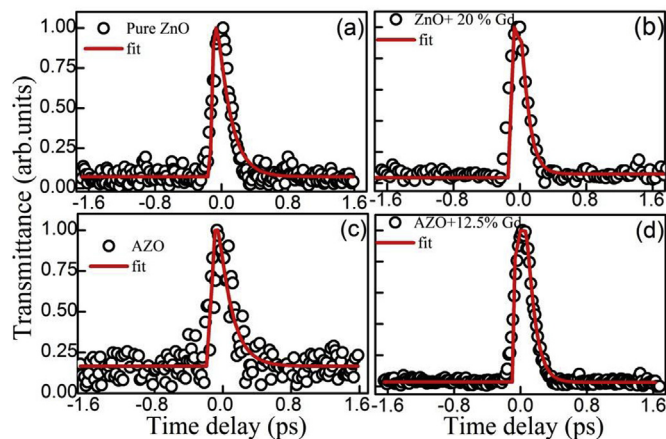


Fig. 7. Transient absorption dynamics of (a) ZnO, (b) ZnO + 20%Gd, (c) AZO, and (d) AZO + 12.5%Gd.

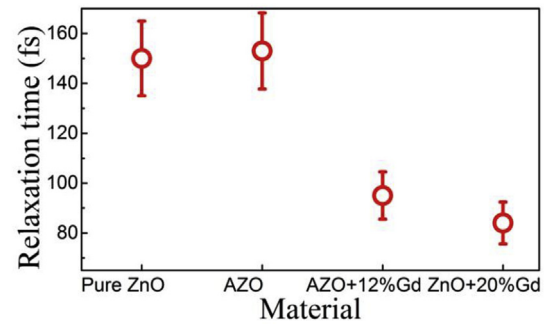


Fig. 8. Relaxation time constants of ZnO and ZAO with different concentrations of Gd.

no influence of Al doping in ZnO, as it was observed in their absorption spectra. The relaxation time for ZnO+20%Gd were faster (85 fs) compared to ZnO (150 fs). Similar trend was observed for Gd doped AZO, which is shown in Fig. 8. This result implies that the increase in Gd concentration for both ZnO and AZO decreases the relaxation time constant.

3.4. HHG in the plasmas produced on different Gd-doped and pure ZnO-based materials

Previous studies of HHG after ablation of different targets have revealed the advantages of such an approach for frequency conversion in the XUV range [27–29]. In earlier studies, the experimental conditions of HHG, in particular, the delay between the heating and driving pulses, were not optimized. To match the propagation of the driving pulse and the highest concentration of the studied group of multi-atomic species, one, therefore, has to use the electronic delay between the heating and the driving pulses. The application of two electronically separated pulses from different lasers synchronized by a digital delay generator allows analyzing the involvement of various components of ablating target on the HHG process. Application of this approach for HHG in multi-component plasmas, alongside with other methods of harmonics enhancement, requires the analysis of the ablated species, to temporally match them with the propagation of driving femtosecond pulses through the plasma.

A search for new applications of different dopants of

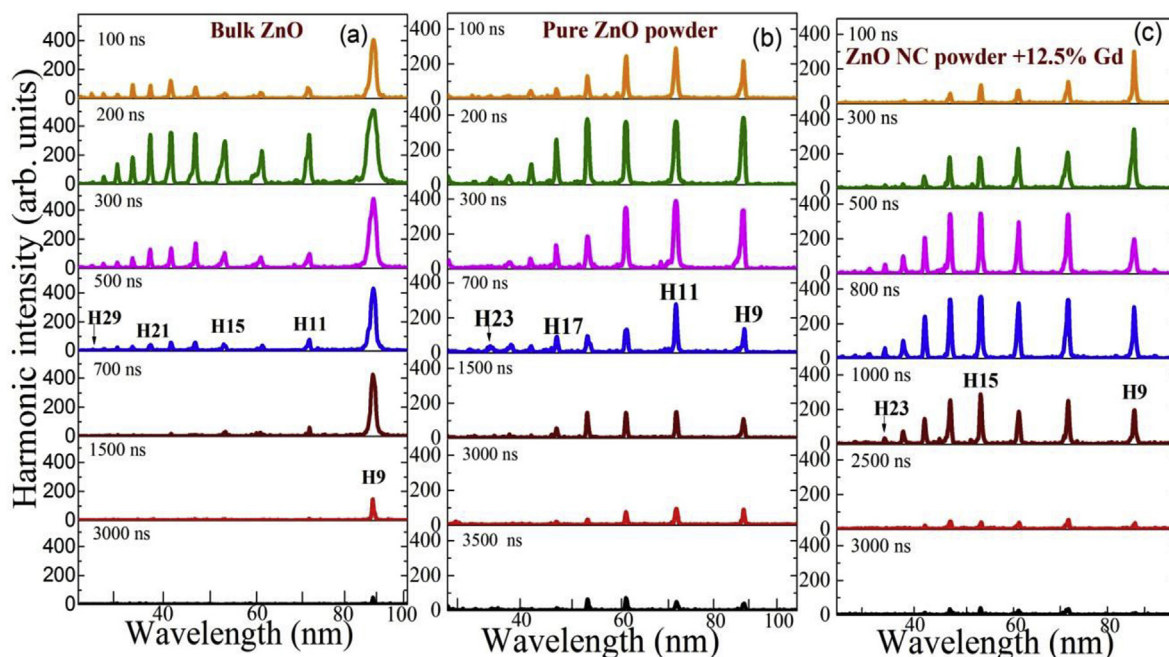


Fig. 9. Harmonics spectra from the ZnO plasmas produced on three targets at different delays between the heating and driving pulses. (a) Bulk ZnO target, (b) Powdered ZnO target. (c) Powdered ZnO doped with 12% weight parts of Gd.

semiconductors is an important problem in optics. The interesting idea is to find the optimal conditions in application of such multi-component structures as effective emitters of the high-order harmonics of femtosecond pulses for the development of efficient sources of coherent XUV radiation. Below we demonstrate HHG in the plasmas produced during ablation of bulk ZnO, ZnO nanocrystal (NC) powder and Gd-doped ZnO NC powder using electronically driven delays between the heating and driving laser pulses. We ablated the samples using nanosecond laser pulses and demonstrated efficient HHG in plasmas using femtosecond laser pulses. Using this approach, we show the influence of Gd on the delay-dependent spectra of harmonics.

Fig. 9 shows high-order harmonics spectra generated from the plasmas produced on the surface of three targets [bulk ZnO, ZnO NC powder and Gd(12% weight ratio)-doped ZnO NC powder] in the spectral range of 25–100 nm. HHG at different delays between the heating and driving pulses (from 100 to 3500 ns) is shown for pulse energies of 4 and 0.8 mJ, respectively. At initial stages of plasma formation and spreading out from the target, i.e., at delays less than 50 ns, the concentration of particles (neutral atoms and molecules and singly charged ions as well as NCs) was insufficient for HHG, since the whole ensemble of particles possessing velocities of $\sim 2 \times 10^4 \text{ m s}^{-1}$ cannot reach the spatial region of the driving beam. At larger delays (100 ns and longer), sufficient amounts of particles appeared in the path of the femtosecond beam that allowed the generation of harmonics. The optimal delay was ~ 200 ns for bulk ZnO, ~ 300 ns for powdered ZnO NCs and ~ 500 ns for Gd-doped ZnO NC powder targets. Gadolinium (atomic weight 157.3 amu) can change the dynamics of delay-dependent harmonics spectra compared with pure ZnO (81.4 amu) target. The harmonics cut-off were similar for two powdered species [Fig. 9(b) and (c)], e.g., at ~ 23 rd harmonic, while ablation of bulk ZnO showed the 29th harmonic as the highest [Fig. 9(a)]. An increase of the delay above the mentioned optimal values led to gradual decrease of HHG efficiency. The harmonics almost disappeared at the delay of 3.5 μs , and no harmonics were observed at delays up to 20 μs .

Experiments using bulk and powdered targets of the same materials led to similar dependencies of the harmonics yield on the delay between the heating and driving pulses. The only difference was the notably strong 9th harmonic in the case of bulk ZnO [Fig. 9(a)]. These

experiments showed that, independently on either molecules or powdered species of ZnO spread out from the target surface, most of them appear in the area of the femtosecond beam approximately at the same time (~ 200 ns).

The harmonics generation in such plasma can check the role of complex composition of ablated species in the former process. A signature revealing the nature of different emitters could be the variation of harmonics emission arising at some specific delay after the beginning of ablation. This delay may characterize the time of propagation of different components from the target's surface to the optical axis of ultrashort pulse propagation. It was suggested in Ref. [30] that if the components could be assumed to reach thermodynamic equilibrium during the expansion, so that a similar average kinetic energy $E = mv^2/2$ could characterize all plasma components, the average arrival times could be assigned to different cluster sizes. The similar assumption can be applied to atoms, molecules and ions of ZnO and Gd. The delay, at which the harmonics reach maximum yield, should scale as a square root of atomic weight. Indeed, as it is shown in present studies, the ejection of heavier atoms and ions (Gd) from the target surface allows them to reach the axis of the driving beam later compared with lighter species (ZnO).

One can expect from the above-mentioned kinetic model the arrival of Gd ions and atoms in the area of interaction with driving beam at $(M_{\text{Gd}}:M_{\text{ZnO}})^{0.5} \sim 1.4$ times later with regard to ZnO particles taking into account the ratio between atomic weights of these two targets ($M_{\text{Gd}}:M_{\text{ZnO}} \approx 2$). Once we compare two similar species (ZnO NC powder doped with Gd and pure ZnO NC powders), the ratio of optimal delays (500 ns: 300 ns ≈ 1.6) is close to the above-mentioned estimates (~ 1.4) based on the kinetic model. Thus, one can assume that this rule works properly for the dynamics of material spreading out from ablation target, once one analyzes the movement of particles during laser ablation at relatively moderate fluencies ($2\text{--}10 \text{ J cm}^{-2}$) of heating nanosecond pulses. These studies showed, for the first time to the best of our knowledge, the influence of dopant in NC-based media on the variation of delay-dependent high-order harmonics spectra produced during propagation of ultrashort laser pulses through the laser-produced plasmas containing ZnO and Gd.

The important peculiarity of this process in three plasmas is a

difference in the variation of harmonics yield for different delays between the heating and driving pulses. Though the same components were used in the case of bulk ZnO and powdered ZnO NCs, the dynamics of plasma formation on these targets causes different harmonics spectra. One can see the strong 9th harmonic in the case of bulk ZnO, which is attributed to the resonance induced enhancement of single harmonic in the vicinity of the ionic transition of Zn possessing large oscillator strength [31]. The enhancement was due to the influence of Zn II resonance (88.1 nm) [32].

Ablation of powdered target requires smaller fluence of heating pulse compared with the ablation of bulk target of similar consistency, which changes the excitation conditions for the ions. Correspondingly, the role of the ionic transition responsible for the 9th harmonic enhancement in the case of strongly excited bulk target has been diminished in the case of ZnO NC powder. In the case of powdered targets [Fig. 9(b) and 9(c)], the insignificant difference between the 9th and the 11th harmonics was observed, contrary to the case of bulk target [Fig. 9(a)].

HHG is very sensitive to different physical processes occurring in the generating medium. The suppression of high-order harmonics occurs through various mechanisms, such as phase mismatch between the interacting waves, limitation in the concentration of emitters, absorbance in the extreme ultraviolet range, etc. Search for new methods allowing the enhancement of the harmonic yield requires application of different concepts, such as quasi-phase matching, resonance enhancement of single harmonic, nanoparticle-induced growth of harmonic efficiency, and application of extended plasmas. A new concept of addition of some components, which enhance the harmonics, can be another method for the suppression of various impeding processes. Application of the targets doped with rare-earth metals can reveal new opportunities in this direction by either in extension in cutoff energy or in enhancement of some harmonic orders due to closeness of some single harmonics with the ionic transitions possessing strong oscillator strength. The particular task of present studies was to analyze the role of such doping component as gadolinium in variation of harmonic spectrum. Overall, while not enhancing harmonic yield and cutoff, the Gd atoms allow demonstrating how heavier species modify the delay-dependent pattern of HHG.

4. Conclusions

We have analyzed different features of Gd-doped ZnO materials. Gd and Al doping of the synthesized ZnO increases the lattice parameter, while Gd doping in AZO significantly decreases the crystalline sizes. From SEM analysis it was observed that Al doping increased the rate of aggregation, forming larger sized clusters. Al and Gd doping of ZnO formed spherical and non-spheroidal particles, respectively. ZnO and AZO exhibited the nonlinear process of 2PA in OA scheme and the combination of nonlinear refraction and nonlinear absorption. At 800 and 400 nm wavelengths, the nonlinear absorption and nonlinear refraction are slightly affected by Gd-doped in ZnO NCs. The nonlinear refraction increased with increase of laser energy for AZO and decreased with the growth of dopant concentration. Growth of Gd concentration in ZnO and AZO decreased the lifetime of carriers. Therefore, the doping of these materials with Gd can be used for fast optical switching devices.

We also reported for the first time, to the best of our knowledge, studies of the influence of dopant in NC-based media on the variation of higher-order harmonics spectra produced during propagation of ultrashort laser pulses through the laser-produced plasmas containing ZnO and Gd. The higher-order harmonics were generated from the ablated ZnO materials and investigated by varying the delay between the heating and fundamental pulses. The strong 9th harmonic was observed in the case of plasmas produced on the bulk ZnO due to the resonance-induced enhancement of single harmonic, whereas in powdered targets (powdered ZnO NCs and ZnO NCs + 12.5% Gd) insignificant difference

between the 9th and the 11th harmonics was observed. We have demonstrated the influence of dopant on the harmonics spectra at different delays between the heating and driving pulses. Overall, we have shown that doping of ZnO materials with Gd caused variation of transient, morphological, low- and high-order nonlinear optical properties of ZnO.

Acknowledgments

The financial support from the National Key Research and Development Program of China (2017YFB1104700, 2018YFB1107202), National Natural Science Foundation of China (Grant Nos.91752025, 61774155 and 11774340), Jilin Provincial Science & Technology Development Project (20180414019GH) and The Key Program of the International Partnership Program of CAS (181722KYSB20160015) is appreciated. R.A.G. thanks the financial support from the Chinese Academy of Sciences President's International Fellowship Initiative (Grant No.2018VSA0001).

References

- [1] P.C. Ray, Size and shape dependent second order nonlinear optical properties of nanomaterials and their application in biological and chemical sensing, *Chem. Rev.* 110 (2010) 5332–5365.
- [2] I. Žutić, J. Fabian, S. Das Sarma, Spintronics: fundamentals and applications, *Rev. Mod. Phys.* 76 (2004) 323–410.
- [3] Y. Wang, G. Zhu, S. Xin, Q. Wang, Y. Li, Q. Wu, C. Wang, X. Wang, X. Ding, W. Geng, Recent development in rare earth doped phosphors for white light emitting diodes, *J. Rare Earths* 33 (2015) 1–12.
- [4] L. Gao, C. Chen, K. Zeng, C. Ge, D. Yang, H. Song, J. Tang, Broadband, sensitive and spectrally distinctive SnS 2 nanosheet/PbS colloidal quantum dot hybrid photo-detector, *Light Sci. Appl.* 5 (2016) e16126.
- [5] S. Abe, J.J. Joos, L.L. Martin, Z. Hens, P.F. Smet, Hybrid remote quantum dot/powder phosphor designs for display backlights, *Light Sci. Appl.* 6 (2017) e16271.
- [6] X. Yang, D. Lenstra, G.D. Khoe, H.J.S. Dorren, Nonlinear polarization rotation induced by ultrashort optical pulses in a semiconductor optical amplifier, *Opt. Commun.* 223 (2003) 169–179.
- [7] Z. Zhang, Q. Liao, Y. Yu, X. Wang, Y. Zhang, Enhanced photoresponse of ZnO nanorods-based self-powered photodetector by piezotronic interface engineering, *Nano Energy* 9 (2014) 237–244.
- [8] J. Du, Q. Liao, M. Hong, B. Liu, X. Zhang, H. Yu, J. Xiao, L. Gao, F. Gao, Z. Kang, Z. Zhang, Y. Zhang, Piezotronic effect on interfacial charge modulation in mixed-dimensional Van der Waals heterostructure for ultrasensitive flexible photo-detectors, *Nano Energy* 58 (2019) 85–93.
- [9] Z. Zhang, Z. Kang, Q. Liao, X. Zhang, Y. Zhang, One-dimensional ZnO nanorod-structure-based optoelectronics, *Chin. Phys. B* 26 (2017) 118102.
- [10] R.A. Ganeev, A. Rysanyansky, A. Stepanov, T. Usmanov, Saturated absorption and reverse saturated absorption of Cu: SiO₂ at $\lambda = 532$ nm, *Phys. Status Solidi B* 241 (2004) R1–R4.
- [11] T. Karali, N. Can, L. Valberg, A. Stepanov, P. Townsend, C. Buchal, R. Ganeev, A. Rysanyansky, H. Belik, M. Jessett, Optical properties and luminescence of metallic nanoclusters in ZnO: Cu, *Phys. B* 363 (2005) 88–95.
- [12] K. Spoorthi, S. Pramodini, I.V. Kityk, M. Abd-Lefdil, M. Sekkati, A.E. Fakir, R. Ashok, S. Ganesh, P. Poornesh, Investigations on nonlinear optical properties of electron beam treated Gd:ZnO thin films for photonic device applications, *Laser Phys.* 27 (2017) 065403.
- [13] S. Dojalisa, N.R. Panda, B.S. Acharya, Effect of Gd doping on structure and photoluminescence properties of ZnO nanocrystals, *Mater. Res. Express* 4 (2017) 114001.
- [14] Z. Zhou, Z.-R. Lu, Gadolinium-based contrast agents for magnetic resonance cancer imaging, *Wiley Interdiscip. Rev.: Nanomed. Nanobiotechnol.* 5 (2013) 1–18.
- [15] T. Grobner, F.C. Prischl, Gadolinium and nephrogenic systemic fibrosis, *Kidney Int.* 72 (2007) 260–264.
- [16] F. Pulizzi, Is it really intrinsic ferromagnetism? *Nat. Mater.* 9 (2010) 956.
- [17] P. Sharma, A. Gupta, K.V. Rao, F.J. Owens, R. Sharma, R. Ahuja, J.M.O. Guillen, B. Johansson, G.A. Gehring, Ferromagnetism above room temperature in bulk and transparent thin films of Mn-doped ZnO, *Nat. Mater.* 2 (2003) 673.
- [18] H. Shi, P. Zhang, S.-S. Li, J.-B. Xia, Magnetic coupling properties of rare-earth metals (Gd, Nd) doped ZnO: first-principles calculations, *J. Appl. Phys.* 106 (2009) 023910.
- [19] G.M. Dalpian, S.-H. Wei, Electron-induced stabilization of ferromagnetism in Ga_{1-x}Gdx N, *Phys. Rev. B* 72 (2005) 115201.
- [20] R. Ewa, O. Wojciech, R. Lidia, Gadolinium as a new emerging contaminant of aquatic environments, *Environ. Toxicol. Chem.* 37 (2018) 1523–1534.
- [21] S. Kobayakawa, Y. Tanaka, A. Ide-Ekessabi, Characteristics of Al doped zinc oxide (ZAO) thin films deposited by RF magnetron sputtering, *Nucl. Instrum. Methods Phys. Res., Sect. B* 249 (2006) 536–539.
- [22] A.B. Ortega, M.A. Carrasco, M.M. Otero, E.R. Lara, E.G. Ramirez, M.I. Castillo, Analytical expressions for z-scan with arbitrary phase change in thin nonlocal

- nonlinear media, *Opt. Express* 22 (2014) 27932–27941.
- [23] M. Sheik-bahae, A.A. Said, E.W. Van Stryland, High-sensitivity, single-beam n_2 measurements, *Opt. Lett.* 14 (1989) 955–957.
- [24] X. Liu, S. Guo, H. Wang, L. Hou, Theoretical study on the closed-aperture Z-scan curves in the materials with nonlinear refraction and strong nonlinear absorption, *Opt. Commun.* 197 (2001) 431–437.
- [25] O.P. Varnavski, T. Goodson, M.B. Mohamed, M.A. El-Sayed, Femtosecond excitation dynamics in gold nanospheres and nanorods, *Phys. Rev. B* 72 (2005) 235405.
- [26] C. Voisin, D. Christofilos, P.A. Loukakos, N. Del Fatti, F. Vallée, J. Lermé, M. Gaudry, E. Cottancin, M. Pellarin, M. Broyer, Ultrafast electron-electron scattering and energy exchanges in noble-metal nanoparticles, *Phys. Rev. B* 69 (2004) 195416.
- [27] R.A. Ganeev, M. Suzuki, M. Baba, M. Ichihara, H. Kuroda, Low- and high-order nonlinear optical properties of BaTiO₃ and SrTiO₃ nanoparticles, *J. Opt. Soc. Am. B* 25 (2008) 325–333.
- [28] R.A. Ganeev, P. Naik, H. Singhal, J. Chakera, M. Kumar, M. Joshi, A. Srivastava, P. Gupta, High-order harmonic generation in carbon-nanotube-containing plasma plumes, *Phys. Rev. A* 83 (2011) 13820.
- [29] R.A. Ganeev, V. Strelkov, C. Hutchison, A. Zaïr, D. Kilbane, M. Khokhlova, J. Marangos, Experimental and theoretical studies of two-color-pump resonance-induced enhancement of odd and even harmonics from a tin plasma, *Phys. Rev. A* 85 (2012) 23832.
- [30] R. de Nalda, M. López-Arias, M. Sanz, M. Oujja, M. Castillejo, Harmonic generation in ablation plasmas of wide bandgap semiconductors, *Phys. Chem. Chem. Phys.* 13 (2011) 10755–10761.
- [31] R.A. Ganeev, Quasi-phase-matching of harmonic waves in plasmas: calculations, new schemes, and applications, *Opt Spectrosc.* 121 (2016) 614–634.
- [32] A.M. Crooker, K.A. Dick, Extensions to the spark spectra of zinc. I. Zinc II and zinc IV, *Can. J. Phys.* 46 (1968) 1241–1251.